

Master's Thesis

Coil Array Inductive Power Transfer System for Autonomous Underwater Vehicle

Yu Cheng

Program of Information Science and Engineering
Graduate School of Information Science
Nara Institute of Science and Technology

Supervisor: Professor Minoru Okada
Network Systems Lab. (Division of Information Science)

January 23, 2021

A Master's Thesis
submitted to Graduate School of Information Science,
Nara Institute of Science and Technology
in partial fulfillment of the requirements for the degree of
MASTER of ENGINEERING

Yu Cheng

Thesis Committee:

Professor Minoru Okada
(Supervisor, Division of Information Science)
Professor Yuichi Hayashi
(Co-supervisor, Division of Information Science)
Associate Professor Takeshi Higashino
(Co-supervisor, Division of Information Science)
Assistant Professor Quang-Thang Duong
(Co-supervisor, Division of Information Science)
Assistant Professor Na Chen
(Co-supervisor, Division of Information Science)

Coil Array Inductive Power Transfer System for Autonomous Underwater Vehicle*

Yu Cheng

Abstract

For a long time, providing a stable, safe, and efficient power supply for underwater electromechanical equipment has always been a concern in deep-sea exploration. Compared with the complicated docking mechanism, potential safety hazards, and expensive price of traditional wet-mate connectors, wireless power transmission (WPT) technology can transmit energy without any electrical contact between the power supply and the electrical equipment, which provides an effective solution to the aforementioned drawbacks of wired charging. There are many uncontrollable factors in the seawater working environment. Therefore, this topic takes the equivalent circuit and magnetic field distribution as the theoretical basis to study the energy transmission characteristics of underwater WPT and proposes corresponding improvements and solutions to the current problems and deficiencies. Especially for the unstable output voltage of the receiver and excessive magnetic flux density at the internal of AUV. This paper proposes a new type of UWPT system with a coil-array structure, which can reduce the magnetic flux density at the center of the AUV by 40% compared to the conventional cylindrical structure.

Keywords:

Autonomous underwater vehicle, inductive power transfer, underwater wireless power transfer, undersea

*Master's Thesis, Graduate School of Science and Technology, Nara Institute of Science and Technology, January 23, 2021.

Contents

| | |
|---|-----------|
| List of Figures | iv |
| List of Tables | vi |
| 1 Introduction | 1 |
| 1.1 Background and research purpose | 1 |
| 1.2 Wireless power transfer technologies | 3 |
| 1.3 Underwater wireless power transfer | 4 |
| 1.3.1 Underwater environment | 5 |
| 1.3.2 Common UWPT systems | 6 |
| 1.4 The main research content of this thesis | 7 |
| 1.5 Roadmap | 7 |
| 2 Basic principles of IPT | 9 |
| 2.1 Inductive coupling model | 9 |
| 2.2 Compensation network technologies | 10 |
| 2.2.1 S-S compensation topology | 11 |
| 2.2.2 CLC-S compensation topology | 12 |
| 2.3 Underwater WPT system model | 13 |
| 3 Preliminary exploration of underwater IPT system | 15 |
| 3.1 The system in three different media | 15 |
| 3.2 The system in different distance | 16 |
| 3.3 The system in different frequency | 19 |
| 3.4 Conclusion | 19 |
| 4 Coil array WPT | 21 |
| 4.1 Measurement of the coil-array WPT system | 22 |

| | | |
|-------------------|--|-----------|
| 4.2 | The other coil arrangements and comparison | 25 |
| 4.3 | Magnetic field distribution | 26 |
| 4.4 | Coil array WPT under seawater | 28 |
| 5 | Conclusion | 30 |
| 5.1 | Future works | 30 |
| References | | 32 |

List of Figures

| | | |
|-----|---|----|
| 1.1 | Underwater sensor networks architecture [1]. | 2 |
| 1.2 | Near-field wireless power transfer. | 4 |
| 1.3 | Far-field wireless power transfer. | 5 |
| 1.4 | Stacked UWPT system [9]. | 6 |
| 1.5 | The primary and secondary coils of stacked UWPT system [9]. | 6 |
| 1.6 | Plug-in UWPT system [13]. | 7 |
| 2.1 | Inductive coupling model. | 9 |
| 2.2 | Equivalent circuit of inductive coupling model. | 10 |
| 2.3 | Compensation networks. | 11 |
| 2.4 | S-S structure. | 12 |
| 2.5 | CLC-S structure. | 13 |
| 2.6 | Equivalent circuit of the coil under seawater. | 14 |
| 3.1 | Two ring structure. | 15 |
| 3.2 | Two ring structure ($r_{inner} = 50mm$, $r_{outer} = 80mm$). | 17 |
| 4.1 | Coil-array structure. | 21 |
| 4.2 | Sechematic diagram of coil-array UWPT system. | 22 |
| 4.3 | Coil-array IPT structure (Both sides with ferrite tile), inner coil in the center or the outer coil. | 23 |
| 4.4 | Measurement of L_s | 23 |
| 4.5 | Equivalent circuit of two coil model. | 24 |
| 4.6 | Coil-array IPT structure (Both sides without ferrite tile), inner coil in the center of the outer coil (Left), inner coil next to the outer coil (Right). | 25 |

| | | |
|------|---|----|
| 4.7 | Coil-array IPT structure (Both sides without ferrite tile), inner coil in the center of the outer coil (Left), inner coil next to the outer coil (Right). | 26 |
| 4.8 | Coil-array IPT structure (Inner small coils with ferrite tile, outer small coils without ferrite tile), inner coil in the center of the outer coil (Left), inner coil next to the outer coil (Right). | 27 |
| 4.9 | Two kind of UWPT coil structure simulation diagram. | 27 |
| 4.10 | Magnetic field distribution of coil-array IPT structure. | 28 |
| 4.11 | Cross-sectional view of the magnetic field distribution of aoil-array IPT structure. | 28 |
| 4.12 | Magnetic field distribution of two ring IPT structure. | 29 |
| 4.13 | Cross-sectional view o f the magnetic field distribution of two ring IPT structure. | 29 |

List of Tables

| | | |
|-----|--|----|
| 1.1 | The different wireless power transmission technologies. | 3 |
| 2.1 | The dielectric constant & conductivity of some materials at 25°C under 1kHz. | 13 |
| 3.1 | The parameters of ring coil structure. | 16 |
| 3.2 | The parameters of ring coil structure. | 17 |
| 3.3 | Z-parameters in different distance and media | 18 |
| 3.4 | The parameters of ring coil structure. | 19 |
| 3.5 | Z-parameters in different frequencies and media | 20 |
| 4.1 | The parameters of coil-array structure. | 22 |
| 4.2 | Maximum power transfer efficiency of different coil arrangements. | 26 |

1 Introduction

1.1 Background and research purpose

In the foreseeable future, the electrification of ocean systems, renewable ocean power sources, and ocean energy networks will be necessary, which will help accelerate the growth and deployment of ocean renewable energy and ways to explore and understand the ocean [8, 10]. To achieve electrification in the ocean, it is necessary to deploy corresponding sensor networks underwater and process the data received by underwater sensors in a timely manner (Figure 1.1). At the same time, underwater sensors are also an essential tool for studying the marine environment [5, 14]. They can easily and flexibly explore underwater terrain and ecological environment, which provides convenience for the deployment of underwater sensor networks. An excellent AUV needs to have good equipment waterproofness, long-distance underwater controllability, and power durability. For the water-resistance of the equipment, we can use high-performance waterproof and pressure-resistant materials [6, 11]. The remote controllability needs to solve the problems of long-distance underwater wireless communication. The durability of electrical equipment requires low energy consumption AUV and high-energy batteries or a continuous power supply. Sufficient power supply can keep underwater sensors and AUVs in an efficient and stable working state for a long time [7]. Indirectly, reducing human interference when electrical equipment is working underwater can also improve work efficiency and reduce deployment costs. Therefore, the energy supply for underwater electrical equipment has become a novel research direction. Such methods can solve the energy supply problem of underwater equipment economically and ensure the system to perform long-term and stable work [3].

In traditional marine engineering, power is supplied to underwater equipment

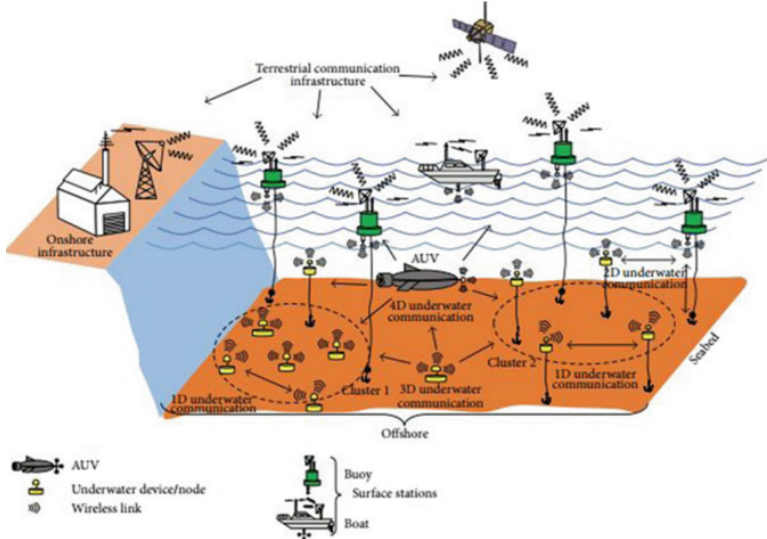


Figure 1.1: Underwater sensor networks architecture [1].

through wet-mate subsea connectors [4]. For the traditional wet plug interface technology, its high cost, complex docking method, poor safety performance, and easy to be corroded by seawater, make its disadvantages in marine engineering increasingly obvious. Wireless Power Transfer (WPT) simplifies the connection between underwater equipment and power supply, reduces the continuous operating cost of underwater equipment, saves a lot of resources, and gradually gains the favor of scholars.

The ocean itself and its surroundings contain a lot of energy, such as tidal energy, wave energy, marine current power, ocean thermal energy, and sea salinity gradient power [2, 4, 12, 15]. Ocean energy is rich, widely distributed, clean, and pollution-free, but low energy density and strong regionality. These advantages make it attractive as grid-connected energy, and may also make it an isolated and remote ocean energy source, thereby providing a valuable source of ocean space. Continuous development provides power solutions that are attractive. The rapid development of distributed ocean energy applications (such as underwater sensor networks, ocean sensors and monitoring technologies, ocean automatic network buoys, and deep-sea and tsunami buoys) is beneficial. In particular, it can power an autonomous underwater vehicle (AUV) whose service life is limited by its battery power.

Table 1.1: The different wireless power transmission technologies.

| Technology | Range | Frequency | Antenna devices | Applications |
|------------|----------|------------|---|--|
| Microwaves | hm – km | GHz | Parabolic dishes, phased arrays, rectennas | Satellite, drone aircraft |
| Optical | dam – km | \geq THz | Lasers, photocells, lenses | Drone aircraft, space elevator |
| Capacitive | cm – m | kHz – MHz | Metal plate electrodes | Smartcards, biomedical implant |
| Inductive | mm – m | Hz – GHz | Tuned wire coils, lumped element resonators | Electric toothbrush, smartphone, electric vehicle |

1.2 Wireless power transfer technologies

Broadly speaking, power transfer without direct electrical contact between the primary and secondary is wireless power transfer. Wireless power technology can be divided into two main categories, near-field (nonradiative region) power transfer and far-field (radiative region) power transfer. Near-field means the area within about 1 wavelength (λ) of the antenna. The range of near-field devices is conventionally divided into two categories [ref] (Suppose the distance between two antennas is represented by D_{range} , and the diameter of two antenna coils is represented by $D_{ant.}$):

- Short range, the distance between two antennas is less than the diameter of antenna: $D_{range} \leq D_{ant.}$. In this range, power is usually transferred through non-resonant capacitive or inductive coupling.
- Mid-range, the distance between two antennas is less than 10 times the diameter of antenna: $D_{range} \leq 10D_{ant.}$. In this range, energy is usually transferred through resonant capacitive or inductive coupling.

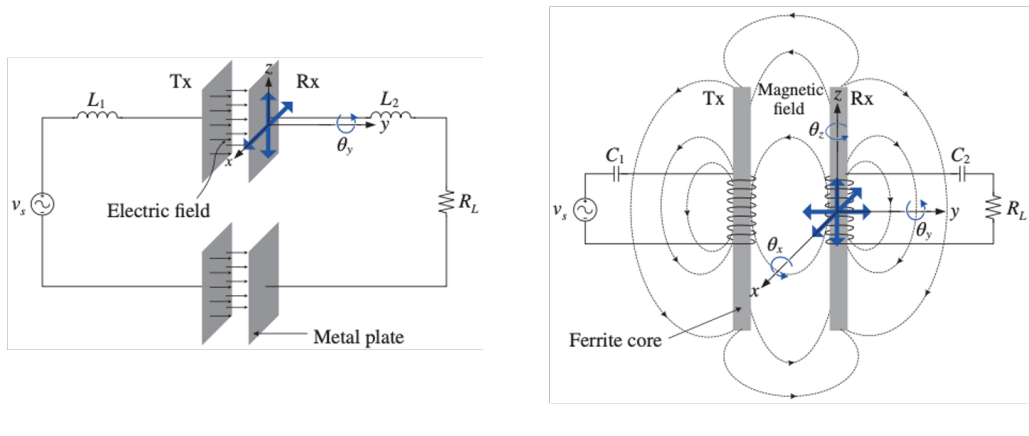
Far-field or radiative region, power is transmitted by means of electromagnetic waves, like radio waves, microwaves, or light waves. When the operating frequency (f) is relatively low, wavelength $\lambda = c/f$, at this time the diameter of the

antenna is much smaller than the wavelength, $D_{ant} \ll \lambda$, and the radiated power will be very small. When the diameter of antenna is about wavelength, $D_{ant} \approx \lambda$, radiate power will be efficient. When the diameter of antenna is much great than wavelength, $D_{ant} \gg \lambda$, we can using high-gain antennas to concentrate electromagnetic waves on a narrow beam and directly aim at the receiver to improve transmission efficiency.

Therefore, near-field wireless power transfer systems mainly include inductive coupling power transfer and capacitive coupling power transfer (Figure 1.2). Far-field wireless power transfer systems mainly include microwave, optical, and acoustic power transfer (Figure 1.3). The respective characteristics are shown in the table 1.1.

1.3 Underwater wireless power transfer

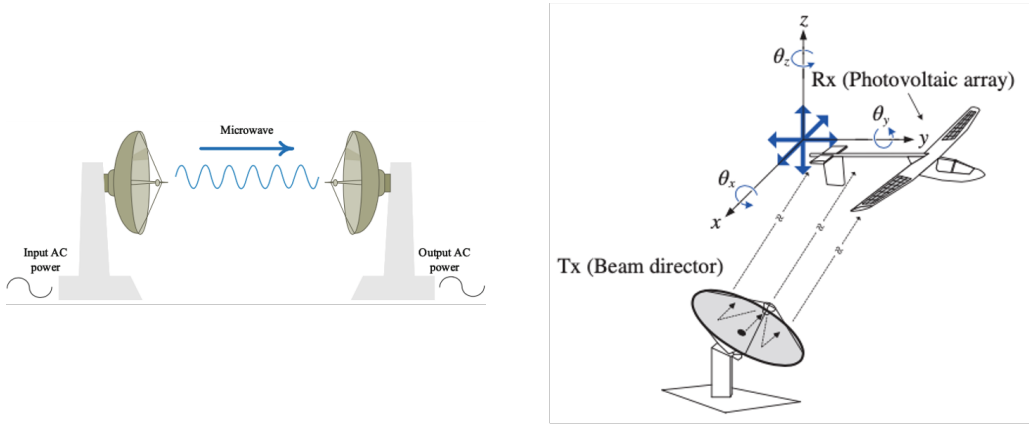
WPT technology has unique advantages in special environments, and along with the continuous development of landing application research and the emergence of a large number of results, it has attracted the attention of underwater technology researchers.



(a) Capacitive power transfer [3].

(b) Inductive power transfer [3].

Figure 1.2: Near-field wireless power transfer.



(a) Microwave power transfer [10].

(b) Laser power transfer [3].

Figure 1.3: Far-field wireless power transfer.

1.3.1 Underwater environment

In the seawater environment, we usually need to consider the following points.

- Underwater, seawater has a blocking effect on high-frequency electromagnetic waves. The distance of electromagnetic waves propagating underwater is inversely proportional to the frequency, making it difficult to achieve long-distance power transmission.
- Conductivity, due to the electrical conductivity of seawater, traditional wireless power transmission analysis methods are no longer applicable. At present, the system modeling and related theoretical analysis of underwater wireless power transfer technology need to be improved.
- Undercurrent, the submarine landform is complex and there is undercurrent. The coupler core is liable to drift under water, and there are problems such as difficulty in docking, which results in low transmission efficiency.
- Some other imprints, like microbial enrichment, temperature, salinity, etc.

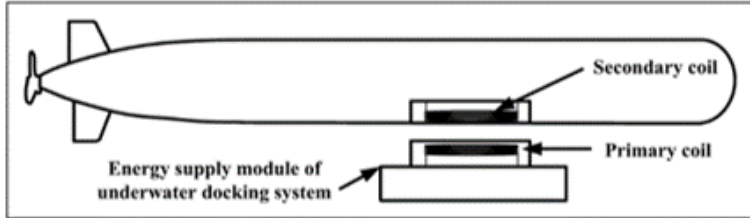


Figure 1.4: Stacked UWPT system [9].

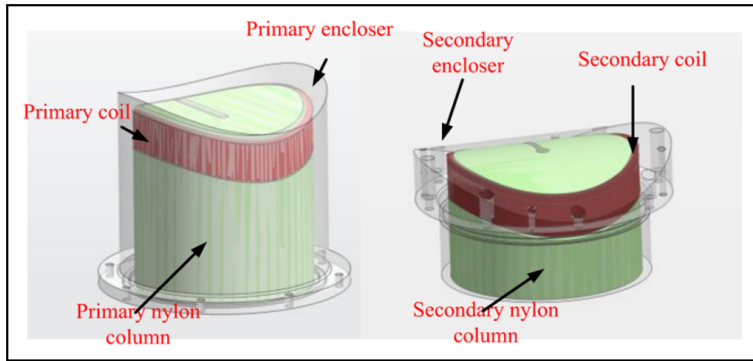


Figure 1.5: The primary and secondary coils of stacked UWPT system [9].

1.3.2 Common UWPT systems

Figure 1.4 shows a stacked UWPT system, this study was completed by Baowei Song et al [9]. They achieved a transmission efficiency of 72% while maintaining 100w output power. They are using a saddle structure transmitter (Details as shown in figure 1.5) and a deformed cylindrical receiver. This structure is very convenient for AUT to park, but because there is no stable protection structure, it is also easy to shift when charging.

Figure 1.6 shows the plug-in UPWT system. We can observe that the AUV needs to be moved into a hollow cylindrical structure transmitter, which makes it difficult to park. However, this structure can maintain the stability of the AUV during AUV charging, so that the system charging is more secure. Another advantage of this structure is that the receiving coil is relatively large, which can make the mutual inductance high. And we can use this system to transmit larger power. Therefore, our coil-array structure UWPT system is built on this structure.

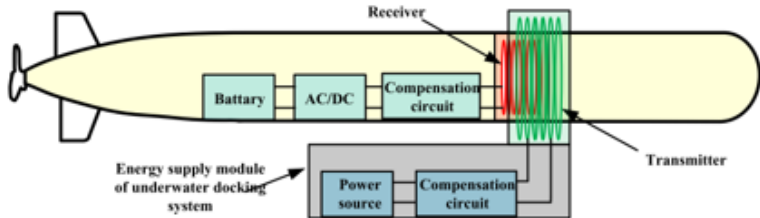


Figure 1.6: Plug-in UWPT system [13].

1.4 The main research content of this thesis

This paper mainly studies the underwater wireless power transfer system, and analyzes the difference between the underwater environment and the land environment WPT system. Considering the durability and high reliability of underwater AUV, this paper proposes a novel coil array power transfer system. It provides reference materials for the subsequent research on the wpt system of multiple coil groups.

1.5 Roadmap

The first chapter analyzes the background of this research and its research purpose and significance, analyzes the characteristics and advantages and disadvantages of mainstream WPT technology, and provides a basis for using IPT technology as an underwater wireless energy transmission system in the following text. A detailed summary and analysis of the current research status of related technologies at home and abroad, including underwater wired energy transmission technology, WPT technology in underwater and air media, and an explanation of the research focus of this article.

The second chapter focuses on the analysis of the basic theory of wireless energy transmission. First, the basic IPT model is explained, and its working principle is analyzed. Then explained the related technology of compensation network. Finally, analyze the underwater IPT system model.

The third chapter initially explores the influence of the underwater environment on the scene wpt system. First, by measuring the Z-parameter in three different media to observe the changes of the wpt system parameters in different media.

Then by changing the size of the internal coil to change the distance between the coils, to judge the change of the wpt system parameters at different distances. Finally, by changing different working frequencies, we can observe the changes of system parameters under different comments.

Chapter four introduces the coil-array coil structure we proposed. The simulation was carried out by Wipl-d software, and the magnetic field distribution and system transmission efficiency of the coil-array coil structure and the two-ring structure were compared. Then through experiments, we compared the performance of several different coil-array arrangements. Summarize the pros and cons of different arrangements.

Chapter five summarizes the experimental results and some shortcomings in the previous article. In response to these shortcomings, some suggestions that can improve the performance of the experiment are put forward, which are written in the future work.

2 Basic principles of IPT

This chapter will first introduce the principle of IPT technology from the physical level, and then introduce the principle of IPT technology from the circuit level, analyze the relationship between different equivalent models, and derive system energy transmission indicators that can represent system performance. And analyze the influence of relevant design parameters on system transmission performance. Analyze the influence of the medium on the system performance in the WPT process, and propose an equivalent model in the underwater working environment. Perform simulation analysis on the derivation to ensure that complete theoretical support is provided for more detailed theoretical research and research on new IPT technology.

2.1 Inductive coupling model

Figure 2.1 depicts the circuit model of IPT systems, where the transmitting coil L₁ and the receiving coil L₂ are directly connected to the power source and the load, respectively. Denote M as the mutual inductance, r₁ and r₂ as the equivalent AC resistance of coils.

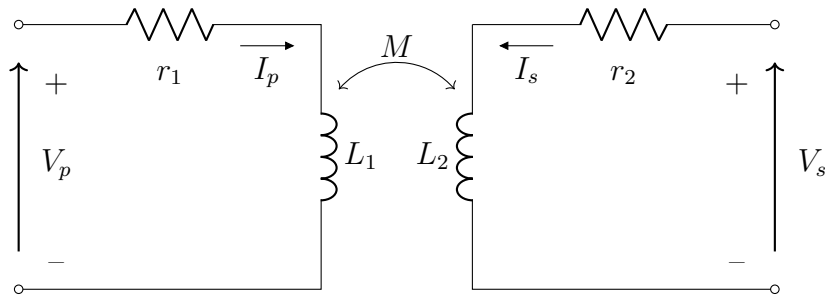


Figure 2.1: Inductive coupling model.

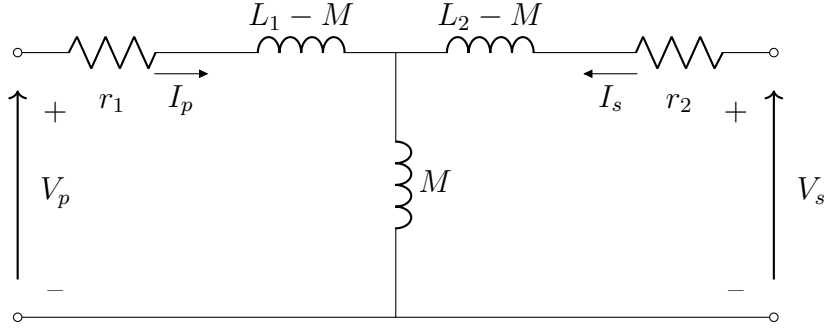


Figure 2.2: Equivalent circuit of inductive coupling model.

Therefore, the equivalent circuit can be expressed as figure 2.2. According to the Kirchhoff's circuit laws. The following formulas can be easily found.

$$V_p = I_p[r_1 + j\omega(L_1 - M)] + (I_p + I_s)j\omega M \quad (2.1)$$

$$= r_1 I_p + j\omega L_1 I_p - j\omega M I_p + j\omega M I_p + j\omega M I_s \quad (2.2)$$

$$= (r_1 + j\omega L_1) I_p + j\omega M I_s \quad (2.3)$$

$$V_s = j\omega M I_p + (r_2 + j\omega L_2) I_s \quad (2.4)$$

The above equations can be expressed as the following matrix equation.

$$\begin{bmatrix} V_p \\ V_s \end{bmatrix} = \begin{bmatrix} r_1 + j\omega L_1 & j\omega M \\ j\omega M & r_2 + j\omega L_2 \end{bmatrix} \begin{bmatrix} I_p \\ I_s \end{bmatrix} \quad (2.5)$$

If we use \mathbf{V} , \mathbf{Z} , \mathbf{I} to express the corresponding matrices. The formula 2.5 can be represented as follows.

$$\mathbf{V} = \mathbf{Z} \cdot \mathbf{I} \quad (2.6)$$

Here, the imaginary part of Z_{11} ($j\omega L_1$) and Z_{22} ($j\omega L_2$) can be canceled by the compensation networks.

2.2 Compensation network technologies

A compensation network is a network that makes some adjustments to compensate for system electrical defects. If capacitor compensation is used only on the

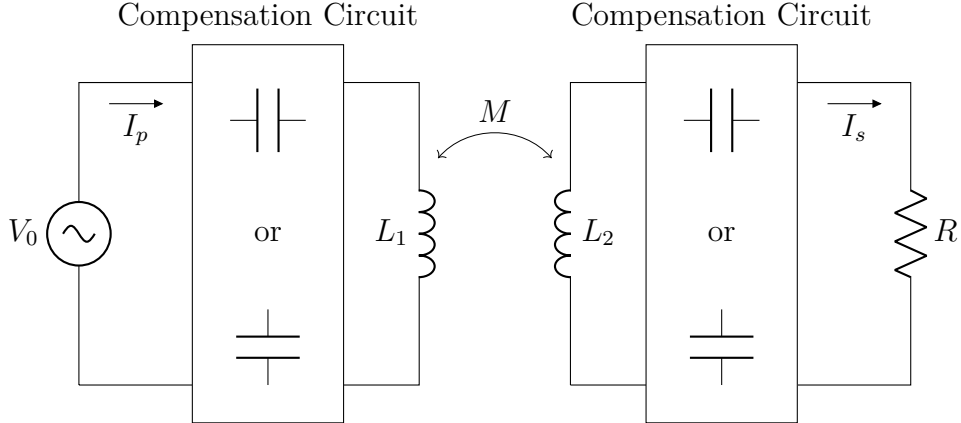


Figure 2.3: Compensation networks.

primary or secondary side, it is called single-sided compensation topology; when capacitor compensation is used on both the primary and secondary sides at the same time, it is called double-sided compensation topology. The calculation of the capacitance value of single-sided compensation is relatively simple, but the actual effect is not as good as the double-sided compensation method. Therefore, this article only discusses bilateral compensation. As shown in the figure 2.3, according to the different connection modes of the capacitors on both sides, common resonance compensation technologies can be divided into four structures: S-S, S-P, P-S, P-P (S denotes series and P denotes parallel). In addition, there are more complicated compensation networks such as CLC and LCC.

Since only S-S topology and CLC-S topology are used in the following text, we only analyze these two compensation topologies in detail here.

2.2.1 S-S compensation topology

When the inductors and the capacitors in the resonance state, we have,

$$\omega = \omega_0 = \frac{1}{\sqrt{LC}}, \quad (2.7)$$

where ω represents the working frequency, ω_0 represents the resonant angular frequency of the circuit. Here, to maximize the transmission efficiency of the WPT system, we need to make the resonant frequencies of the primary side and

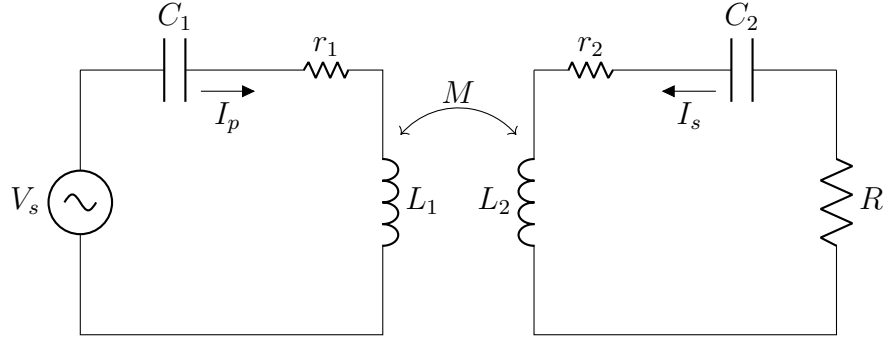


Figure 2.4: S-S structure.

secondary side consistent. Therefore,

$$\omega_0 = \frac{1}{L_1 C_1} = \frac{1}{L_2 C_2} \quad (2.8)$$

For any formed coil, we can measure its corresponding inductance value at a specified frequency. Thus, we can get the value of the compensation capacitor by formula 2.7.

$$C = \frac{1}{\omega_0^2 L} \quad (2.9)$$

$$k = \frac{M}{\sqrt{L_1 L_2}} \quad (2.10)$$

2.2.2 CLC-S compensation topology

$$V_S = -j X_C I_S + j X_L I_L \quad (2.11)$$

$$V_0 = (-j X_{C_0} + j X_{L_0} + r_0) I_0 + j \omega M I_1 \quad (2.12)$$

$$V_R = j \omega I_0 + (-j X_{C_1} + j X_{L_1} + r_1) I_1 \quad (2.13)$$

$$V_R = -R I_1 \quad (2.14)$$

$$I_S = I_L + I_0 \quad (2.15)$$

$$V_R = -\frac{R}{R + r_1} \cdot \frac{\omega M}{X_L} V_S \quad (2.16)$$

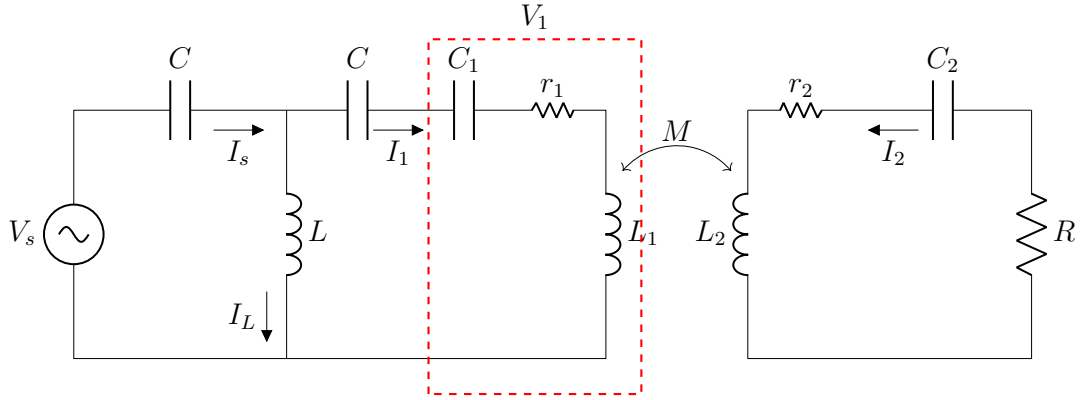


Figure 2.5: CLC-S structure.

2.3 Underwater WPT system model

In the seawater environment, the electrical parameters of seawater as the transmission medium are quite different from those in the air, as shown in the table 2.1.

Table 2.1: The dielectric constant & conductivity of some materials at 25°C under 1kHz.

| Material | Relative permittivity | Conductivity |
|------------------|-----------------------|--------------------------|
| Vacuum | 1 | 0 S/m |
| Air | 1.0006 | 0 S/m |
| Ultra pure water | 81 | 5.5×10^{-6} S/m |
| Drinking water | 81 | 0.005 – 0.05 S/m |
| Seawater | 81 | 5 S/m |

It can be seen from table 2.1 that the relative permittivity of seawater is larger than that of air medium, resulting in a distributed capacitance between two conductors that are relatively close in seawater; at the same time, seawater has a certain conductivity , This is equivalent to connecting an eddy current loss resistor in series at both ends of the coil. Eddy current loss resistance and distributed capacitance will affect the impedance of the coil and generate additional power loss. Therefore, the conventional mutual inductance model of formula 2.5. cannot

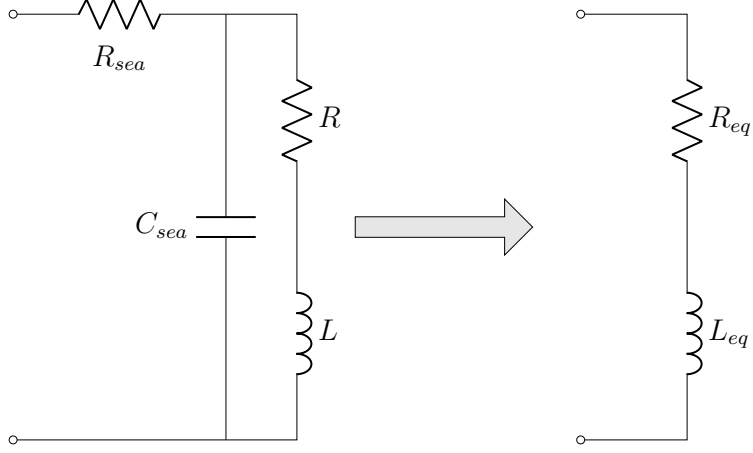


Figure 2.6: Equivalent circuit of the coil under seawater.

reflect the influence of seawater media on transmission, and cannot completely and accurately describe the transmission behavior under seawater.

As shown in figure 2.6, R_{sea} is the eddy current loss resistance, C_{sea} is the distributed capacitance, both of which increase with the increase of operating frequency, R is the internal resistance of the coil itself, and L is the coil inductance. The mathematical expressions of equivalent inductance L_{eq} and equivalent resistance R_{eq} are as follows,

$$L_{eq} = \frac{L - \omega^2 L^2 C_{sea} - C_{sea} R^2}{(1 - \omega^2 L C_{sea})^2 + \omega^2 C_{sea}^2 R^2}, \quad (2.17)$$

and

$$R_{eq} = R_{sea} + \frac{R}{(1 - \omega^2 L C_{sea})^2 + \omega^2 C_{sea}^2 R^2}. \quad (2.18)$$

Where ω is the operating angular frequency. Generally speaking, eddy current loss resistance R_{sea} and distributed capacitance C_{sea} are affected by many factors and are difficult to measure. Therefore, equations 2.17 and 2.18 are not easy to calculate, and they are usually obtained with three-dimensional electromagnetic field simulation software or experiments. Since R_{eq} is generally larger at high frequencies, underwater magnetic coupling resonance wireless energy transmission generally uses a working frequency below 1 MHz.

3 Preliminary exploration of underwater IPT system

In order to explore the similarities and differences between the wireless energy transmission system in the seawater environment and the wireless energy transmission system in the air in the actual situation, a simple double-coil structure is used to explore the electrical properties of the underwater environment. This chapter will introduce the performance of the double coil structure working in sea water.

3.1 The system in three different media

In order to design a wireless power transmission system suitable for underwater AUV, we will first use hollow cylindrical structure transmitter and cylindrical



(a) Experimental coil.



(b) Structure diagram.

Figure 3.1: Two ring structure.

Table 3.1: The parameters of ring coil structure.

| Items | Parameters |
|-----------------------------------|--------------------------|
| Environment | Air, tap water, seawater |
| Wire diameter | 0.8mm |
| Wire material | Copper |
| Tx coil diameter | 113mm |
| Rx coil diameter | 85mm |
| Turns (Inner coil and outer coil) | 10 |
| Frequency | 200kHz |

structure receiver to explore the performance of the UWPT system of this plug-in structure UWPT in water. For the convenience of writing, it will be referred to as a double ring structure in the following text. The coil structure as shown in figure 4.9.

Its detailed parameters are shown in Table 3.1.

When we use the VNA analyzer to place the coil in the air, tap water, or seawater for measurement, the following data can be obtained:

$$Z_{air} = \begin{bmatrix} 0.4 + 29.6i & 0.0 - 10.0i \\ 0.0 - 10.0i & 0.3 + 20.3i \end{bmatrix},$$

$$Z_{tap-water} = \begin{bmatrix} 3.0 + 32.1i & -1.5 - 11.3i \\ -1.5 - 11.3i & 1.5 + 21.6i \end{bmatrix},$$

$$Z_{seawater} = \begin{bmatrix} 7.2 + 37.8i & -6.0 - 15.7i \\ -6.0 - 15.7i & 6.5 + 25.3i \end{bmatrix}.$$

In the above measurement results, we can find that as the transmission medium changes (From air to tap-water to seawater), each corresponding value is increasing.

3.2 The system in different distance

In order to explore the influence of the size of the internal coil and the distance between the two coils on the system (Figure 3.2), the coil size is changed here

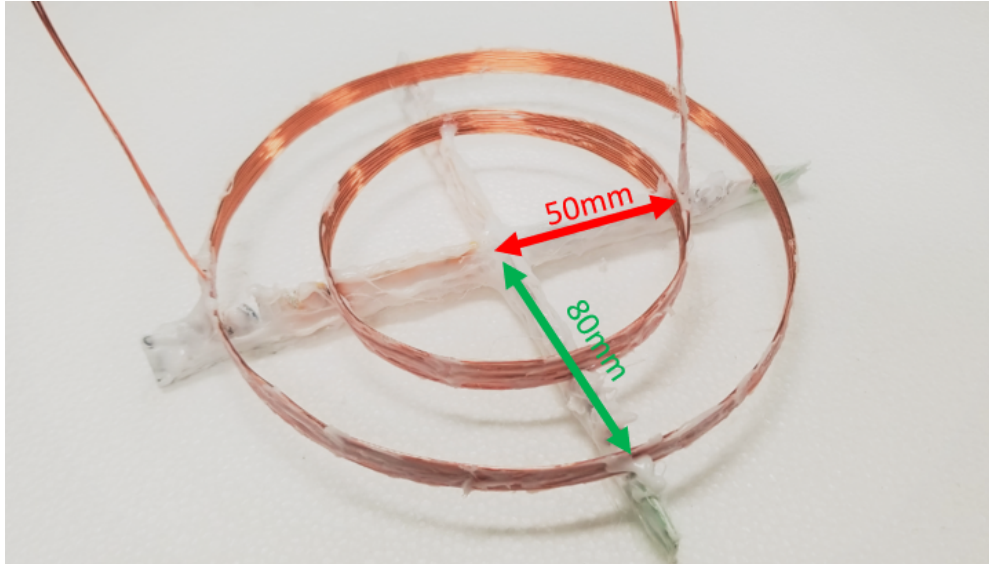


Figure 3.2: Two ring structure ($r_{inner} = 50\text{mm}$, $r_{outer} = 80\text{mm}$).

to change the distance between the transmitter and the receiver. The specific parameters are as follows (Table 3.2).

Table 3.2: The parameters of ring coil structure.

| Items | Parameters |
|-----------------------------------|--------------------------|
| Environment | Air, tap water, seawater |
| Wire diameter | 0.8mm |
| Wire material | Copper |
| Tx coil diameter | 160mm |
| Rx coil diameter | 100mm, 120mm, 140mm |
| Turns (Inner coil and outer coil) | 10 |
| Frequency | 200kHz |

After changing the medium between the coils and the distance between the coils, the Z-parameters in different scenarios are measured by VNA, and we get the following results (Table 3.3).

In table 3.3, we can find that under the same medium, as the internal coil decreases, the transmission distance increases. We can see that the imaginary

Table 3.3: Z-parameters in different distance and media

| Media | Coil size (Radius) | Distance | Z-parameter |
|-----------|-----------------------|----------|--|
| Air | 80mm - 50mm | 30mm | $\begin{bmatrix} 0.6826 + 46.4075i & -0.0411 - 8.9620i \\ -0.0382 - 8.9669i & 0.3423 + 24.2260i \end{bmatrix}$ |
| | 80mm - 60mm | 20mm | $\begin{bmatrix} 0.7194 + 46.1416i & -0.0946 - 15.0048i \\ -0.0906 - 15.0155i & 0.5225 + 32.5246i \end{bmatrix}$ |
| | 80mm - 70mm | 10mm | $\begin{bmatrix} 0.6657 + 45.9561i & 0.0757 + 24.2562i \\ 0.0699 + 24.2747i & 0.5651 + 39.2948i \end{bmatrix}$ |
| Tap-water | 80mm - 50mm | 30mm | $\begin{bmatrix} 5.4603 + 53.0814i & -2.4332 - 11.7753i \\ -2.4304 - 11.7859i & 1.7722 + 26.0449i \end{bmatrix}$ |
| | 80mm - 60mm | 20mm | $\begin{bmatrix} 7.0513 + 54.2993i & -4.4889 - 20.1926i \\ -4.4867 - 20.2100i & 3.9114 + 36.7652i \end{bmatrix}$ |
| | 80mm - 70mm | 10mm | $\begin{bmatrix} 2.8768 + 49.8765i & 0.9991 + 26.5644i \\ 0.9946 + 26.5864i & 1.9865 + 42.0751i \end{bmatrix}$ |
| Seawater | 80mm - 50mm | 30mm | $\begin{bmatrix} 1.761 + 58.2022i & -0.554 - 14.5303i \\ -0.5512 - 14.5424i & 0.6543 + 27.6708i \end{bmatrix}$ |
| | 80mm - 60mm | 20mm | $\begin{bmatrix} 2.0488 + 61.1579i & -0.9906 - 25.1528i \\ -0.9814 - 25.1736i & 1.2212 + 40.4982i \end{bmatrix}$ |
| | 80mm - 70mm | 10mm | $\begin{bmatrix} 2.0347 + 52.4298i & 0.4957 + 27.1092i \\ 0.4843 + 27.1321i & 1.4439 + 43.4828i \end{bmatrix}$ |

part of Z_{11} and Z_{22} are increasing, indicating that the impedance of the coil is increasing.

Table 3.4: The parameters of ring coil structure.

| Items | Parameters |
|-----------------------------------|--|
| Environment | Air, seawater |
| Wire diameter | 0.8mm |
| Wire material | Copper |
| Tx coil diameter | 160mm |
| Rx coil diameter | 100mm |
| Turns (Inner coil and outer coil) | 10 |
| Frequency | 100kHz, 150kHz, 200kHz, 250kHz, 300kHz |

3.3 The system in different frequency

Earlier we have studied the z-parameter changes of the two ring coil structure under different media and different distances. In this section we will study how z-parameters changes at different frequencies. Table 3.4 a shows the parameters of the experiment.

After using the above parameters, we got the following results (Table 3.3).

3.4 Conclusion

Table 3.5: Z-parameters in different frequencies and media

| Media | Frequency | Z-parameter |
|----------|-----------|--|
| Air | 100kHz | $\begin{bmatrix} 0.3758 + 23.2130i & -0.0036 - 4.4495i \\ -0.0012 - 4.4520i & 0.2123 + 12.1526i \end{bmatrix}$ |
| | 150kHz | $\begin{bmatrix} 0.4789 + 34.7320i & -0.0074 - 6.6739i \\ -0.0037 - 6.6774i & 0.2575 + 18.1971i \end{bmatrix}$ |
| | 200kHz | $\begin{bmatrix} 0.5755 + 46.2288i & -0.0121 - 8.9004i \\ -0.0050 - 8.9065i & 0.3031 + 24.2211i \end{bmatrix}$ |
| | 250kHz | $\begin{bmatrix} 0.6737 + 57.7432i & -0.0153 - 11.1342i \\ -0.0095 - 11.1426i & 0.3423 + 30.2465i \end{bmatrix}$ |
| | 300kHz | $\begin{bmatrix} 0.7556 + 69.2691i & -0.0191 - 13.3746i \\ -0.0100 - 13.3859i & 0.3791 + 36.2676i \end{bmatrix}$ |
| Seawater | 100kHz | $\begin{bmatrix} 0.5314 + 24.3255i & -0.0760 - 4.9832i \\ -0.0717 - 4.9862i & 0.2593 + 12.5247i \end{bmatrix}$ |
| | 150kHz | $\begin{bmatrix} 0.9900 + 39.2700i & -0.2453 - 8.8345i \\ -0.2392 - 8.8400i & 0.4080 + 19.6434i \end{bmatrix}$ |
| | 200kHz | $\begin{bmatrix} 2.0236 + 59.0193i & -0.7053 - 15.0451i \\ -0.6942 - 15.0581i & 0.7248 + 28.1895i \end{bmatrix}$ |
| | 250kHz | $\begin{bmatrix} 4.8486 + 89.4034i & -2.0763 - 26.6084i \\ -2.0597 - 26.6276i & 1.5345 + 39.8440i \end{bmatrix}$ |
| | 300kHz | $10^2 \times \begin{bmatrix} 0.1548 + 1.4909i & -0.0751 - 0.5327i \\ -0.0749 - 0.5333i & 0.0450 + 0.5985i \end{bmatrix}$ |

4 Coil array WPT

Through the explanation in the previous chapter, we know the basic performance of the wireless transmission system underwater. This chapter will introduce the underwater coil-array WPT system we designed, by degrading a large double coil structure into multiple small coil structures, as shown in figure 4.1. This greatly reduces the magnetic field in the internal coil, thereby achieving electromagnetic protection inside the AUV system. Its detailed parameters are shown in table 4.1.

In the marine environment, we can use buoys to generate electricity [10], store the collected electricity in the power source, and then connect the power source to the transmitter (Tx). When the AUV (Rx) reaches the designated position of the transmitter, the AUV can be charged wirelessly. This is the basic workflow of this UWPT system. Figure 4.2 shows a schematic diagram of the UWPT system.

In the following subsections, the performance of the coil-array UWPT system

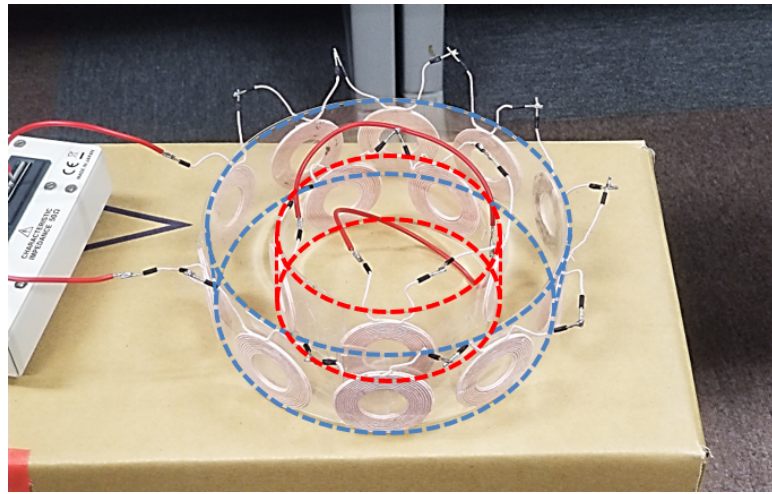


Figure 4.1: Coil-array structure.

Table 4.1: The parameters of coil-array structure.

| Items | Parameters |
|------------------------|--------------------------|
| Tx coil diameter | 160mm |
| Rx coil diameter | 100mm |
| The number of Tx coils | 10 |
| The number of Rx coils | 5 |
| Coil connection | In series |
| Coil model | WE 760308110 (Litz wire) |

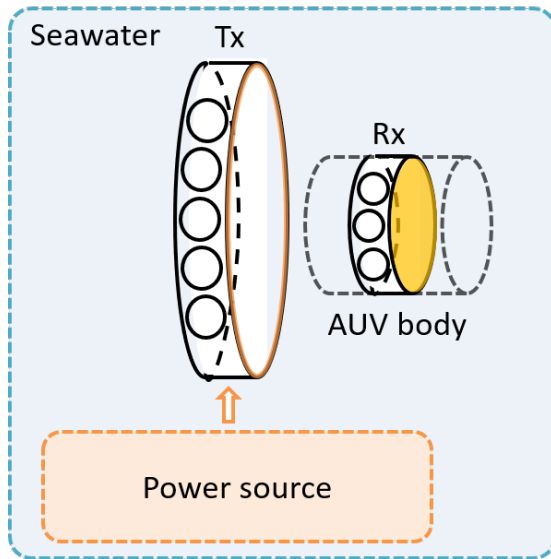


Figure 4.2: Sechematic diagram of coil-array UWPT system.

will be described in detail.

4.1 Measurement of the coil-array WPT system

In this section, we will first introduce different coil arrangements. By changing the coil structure of the coil-array, observe the performance of the changed coil structure under different conditions.

As shown in figure 4.3, a transmitter coil with a radius of 80mm is used here, which consists of 10 coils with ferrite in series, and a receiver coil with a radius



| Parameters | | Inner coil (Tx) | Outer coil (Rx) |
|------------------------|---|-----------------|-----------------|
| Diameter | | 100mm | 160mm |
| Number of coils | | 5 | 10 |
| Material | | Litz wire (2mm) | Litz wire (2mm) |
| 200kHz | Q | 207 | 206.25 |
| | L | $125.01\mu H$ | $241.03\mu H$ |
| Position of inner coil | | center | |
| L_s | | $240.65\mu H$ | |
| M | | 6.8923 | |
| k | | 0.0397 | |
| kQ | | 8.2007 | |
| η_{max} | | 78.41% | |

Figure 4.3: Coil-array IPT structure (Both sides with ferrite tile), inner coil in the center or the outer coil.

of 50mm, which consists of 5 coils with ferrite in series. Therefore, the distance between Tx and Rx is 30mm. For other specific parameters, please find in the figure 4.3.

By using LCR meter to measure this arrangement system, we can get the inductance of the Tx's coil-array coil, $L_1 = 241.03\mu H$, and quality factor $Q_1 = 206.25$. And the inductance of Rx's coil-array coil, $L_2 = 125.01\mu H$, and quality factor $Q_2 = 207$. Then short-circuit the Rx coil and place it in the middle of the Tx coil, and measure the inductance of the Tx in this state (As shown in figure 4.4), which is L_s , where $L_s = 240.65\mu H$.

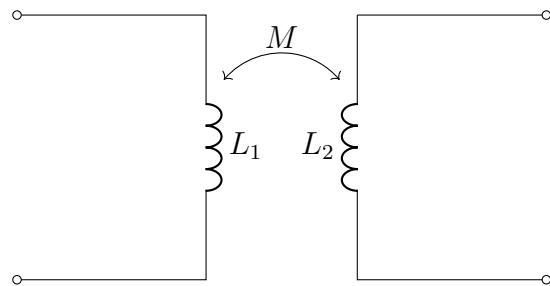


Figure 4.4: Measurement of L_s .

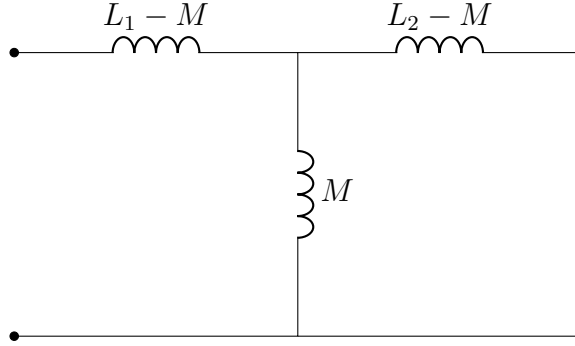


Figure 4.5: Equivalent circuit of two coil model.

From equivalent circuit (Figure 4.5), we can get the following formula.

$$L_s = L_1 - M + \frac{M(L_2 - M)}{L_2}. \quad (4.1)$$

Move M to the left side of the equation, the mutual inductance can be expressed as,

$$M = \sqrt{L_2(L_1 - L_s)}, \quad (4.2)$$

and coupling coefficient,

$$k = \frac{M}{L_1 L_2}. \quad (4.3)$$

kQ product can be expressed as,

$$kQ = k\sqrt{Q_1 Q_2}. \quad (4.4)$$

kQ product is an index showing the performance of a wireless transfer. The relationship between the maximum transmission efficiency η_{max} and kQ as follows \$refLi2015,

$$\eta_{max} = \frac{k^2 Q_1 Q_2}{(1 + \sqrt{1 + k^2 Q_1 Q_2})^2}. \quad (4.5)$$

According to the calculation of the above formula, we can get that the maximum transmission efficiency η_{max} of this arrangement is 78.41%.

4.2 The other coil arrangements and comparison

Next, we will observe the performance of the system under different conditions by increasing the number of coils and changing the position of the Rx coil in the Tx coil. The result is shown in the figure 4.6, figure 4.7, and figure 4.8.

Through the results under each of the above scenarios, we can summarize them into table 4.2, as follows

From table 4.2, we can get the following conclusions:

- When we increase the number of inner coils, the maximum PTE (Power transfer efficiency) will increase.
- If the numbers of outer and inner coils are the same, when outer coils without ferrite and inner coils with ferrite, we can get the maximum PTE.
- When there is no ferrite outside the inner coil, the PTE will increase if the inner coil deviates from the middle, and vice versa.

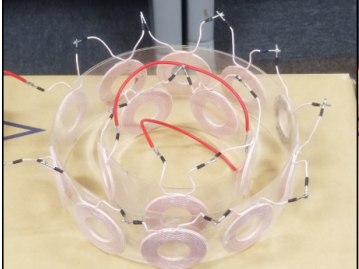
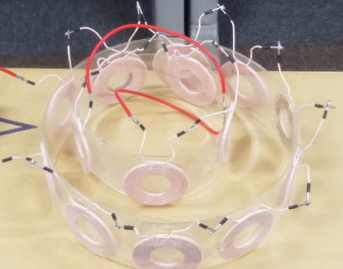
| Number of outer coils | | Number of inner coils | |
|---|--|-----------------------|---------|
| 10 | 5 | | |
|  |  | | |
| M | 4.2371 | M | 8.9941 |
| k | 0.0428 | k | 0.0909 |
| kQ | 7.5365 | kQ | 15.9979 |
| η_{max} | 76.75% | η_{max} | 88.26% |

Figure 4.6: Coil-array IPT structure (Both sides without ferrite tile), inner coil in the center of the outer coil (Left), inner coil next to the outer coil (Right).

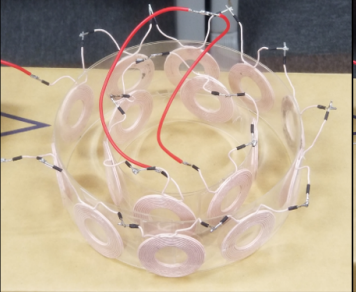
| Number of outer coils | | Number of inner coils | |
|---|--|-----------------------|---------|
| 10 | 6 | | |
|  |  | | |
| M | 4.7709 | M | 13.4385 |
| k | 0.0446 | k | 0.1255 |
| kQ | 7.6436 | kQ | 21.5303 |
| η_{max} | 77.03% | η_{max} | 91.13% |

Figure 4.7: Coil-array IPT structure (Both sides without ferrite tile), inner coil in the center of the outer coil (Left), inner coil next to the outer coil (Right).

4.3 Megnetic field distribution

In order to clarify the magnetic field distribution of the coil-array structure, we used Wipl-d electromagnetic simulation software. We simulated the following two

Table 4.2: Maximum power transfer efficiency of different coil arrangements.

| Shift | Numbers of coil (Outer - Inner) | Both coils with ferrite | Both coils without ferrite | Outer coils without ferrite, inner coils with ferrite |
|----------------------------------|---------------------------------|-------------------------|----------------------------|---|
| Inner coil in the center | 10 - 5 | 78.41% | 76.75% | 84.95% |
| | 10 - 6 | | 77.03% | |
| Inner coil close to the one side | 10 - 5 | | 88.26% | 78.80% |
| | 10 - 6 | | 91.13% | |

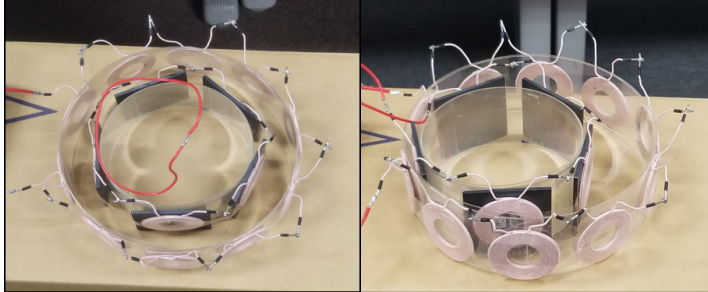
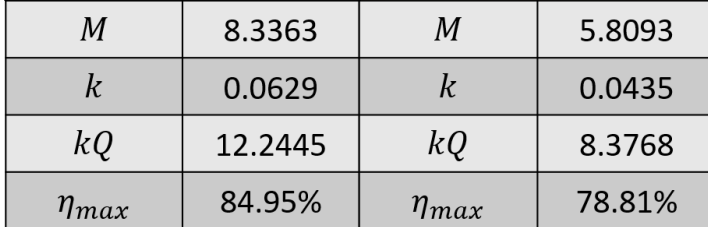
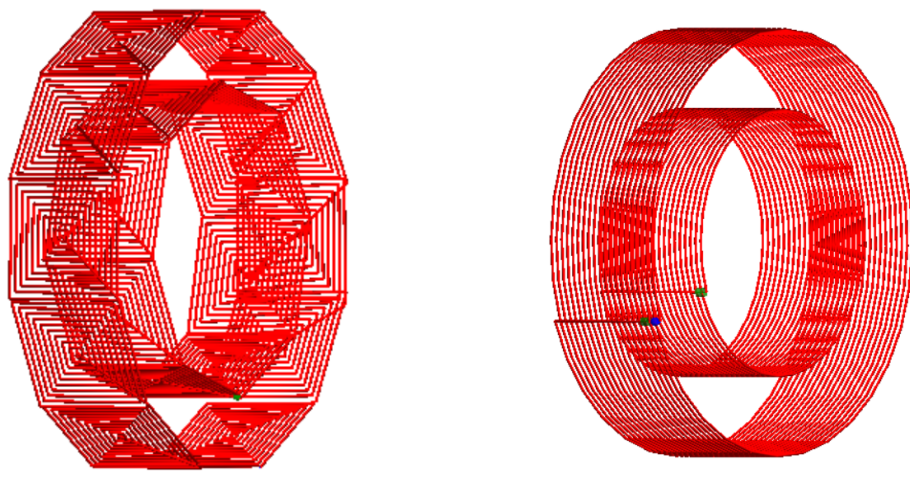
| Number of outer coils | Number of inner coils |
|--|--|
| 10 | 5 |
|  |  |
| M | 8.3363 |
| k | 0.0629 |
| kQ | 12.2445 |
| η_{max} | 84.95% |
| M | 5.8093 |
| k | 0.0435 |
| kQ | 8.3768 |
| η_{max} | 78.81% |

Figure 4.8: Coil-array IPT structure (Inner small coils with ferrite tile, outer small coils without ferrite tile), inner coil in the center of the outer coil (Left), inner coil next to the outer coil (Right).



(a) Coil-array IPT structure.

(b) Two ring IPT structure.

Figure 4.9: Two kind of UWPT coil structure simulation diagram.

structures, and the specific parameters are as follows.

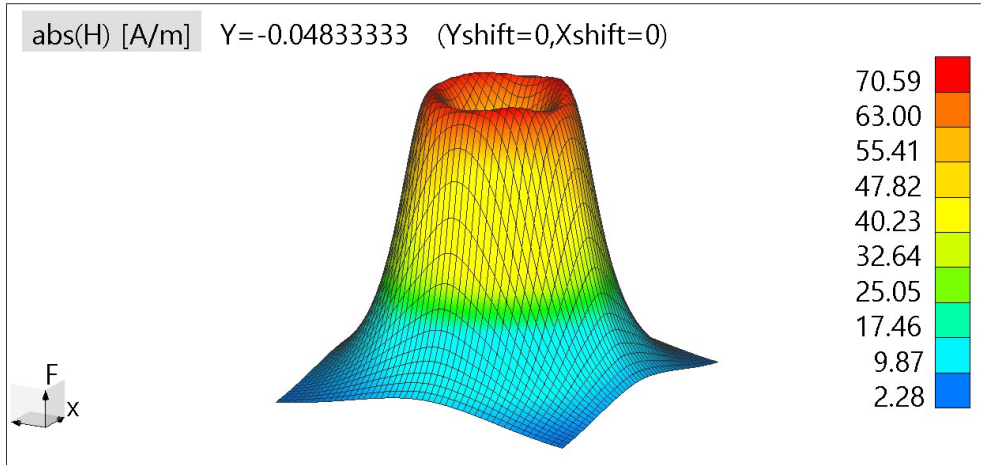


Figure 4.10: Magnetic field distribution of coil-array IPT structure.

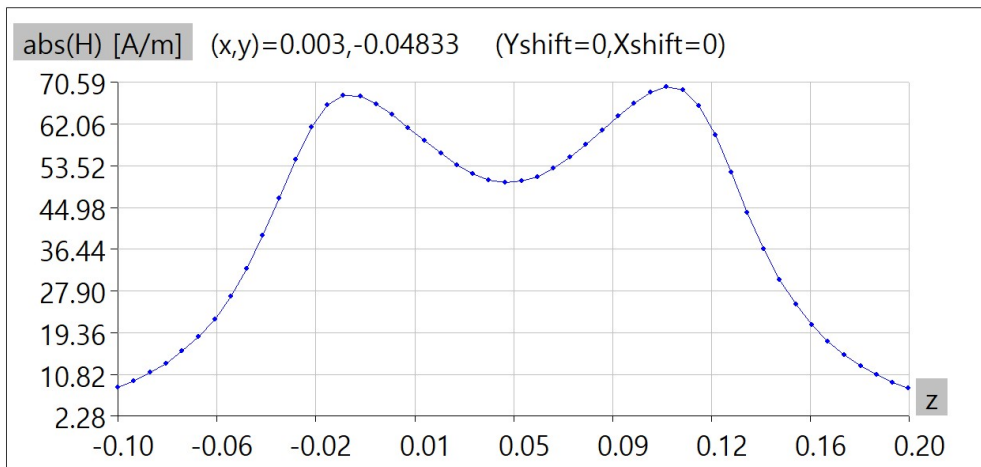


Figure 4.11: Cross-sectional view of the magnetic field distribution of a coil-array IPT structure.

Therefore, we have obtained the magnetic field distribution diagrams of the two coil structures, as follows,

4.4 Coil array WPT under seawater

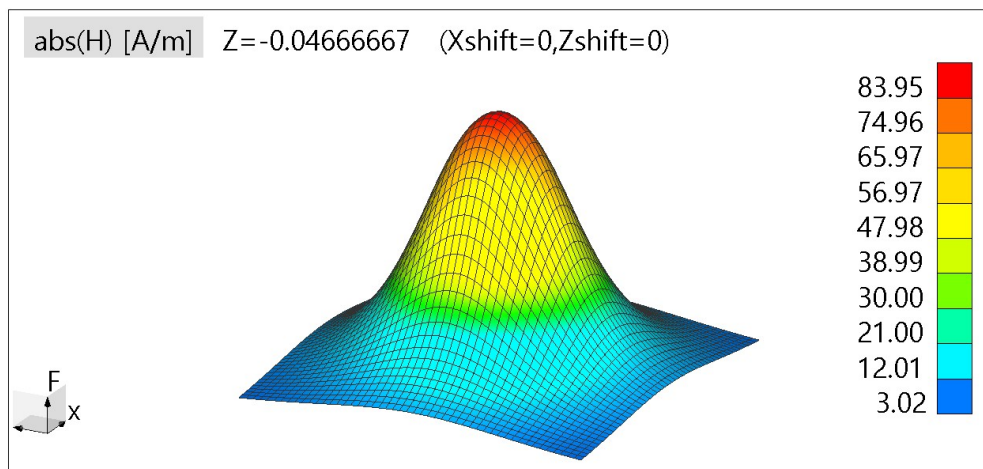


Figure 4.12: Magnetic field distribution of two ring IPT structure.

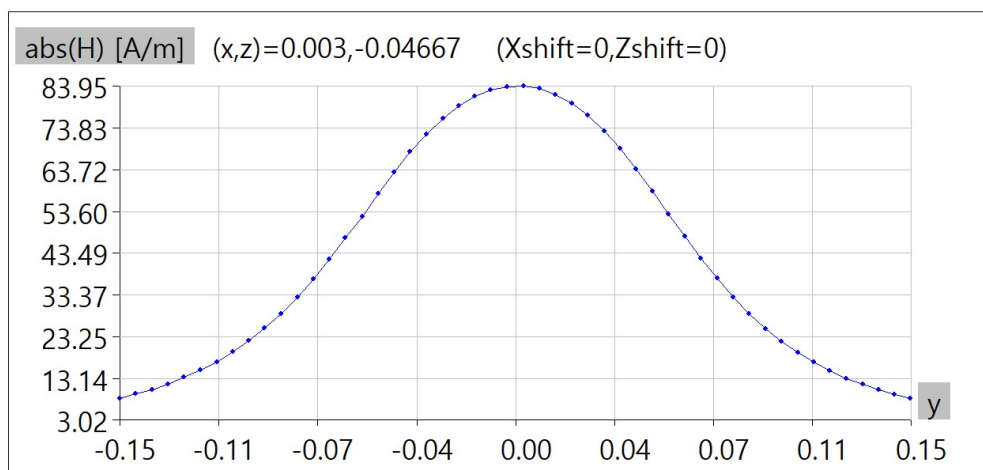


Figure 4.13: Cross-sectional view o f the magnetic field distribution of two ring IPT structure.

5 Conclusion

5.1 Future works

Acknowledgements

First of all, I would like to thank my supervisor, Professor Minoru Okada. Professor Okada is kind, knowledgeable, and rigorous in scientific attitude. Thank him for giving me an opportunity to study in Japan and let me do wireless power transfer research that I am interested in. He has continued to help me during my three years of study and life. At the same time, I would like to thank Professor Yuichi Hayashi for my research advice and guidance, so that I have a deeper understanding of the weak research environment. With his help, Which greatly improved my research.

Then I would like to thank Associate Professor Takeshi Higashino and Assistant Professor Duong Quang Thang. With their help, they have made me better understand the knowledge of wireless power transfer and wireless communication, and they have helped me overcome the difficulties in professional understanding and helped me complete this topic. Thank them very much. Here, I would also like to thank Assistant Professor Chen Na for her continuous help and encouragement in my studies, so that I have a better understanding of the field of communication.

I would also like to thank the members, staff, and seniors of the Network Systems Laboratory for their companionship in the study and life. We studied together and played together, and established a strong friendship together. Thank you to the international students who have helped me while studying abroad. Thank you for your kindness to me.

Finally, I would like to thank my family for their support of studying abroad, let me choose the knowledge I like, and always provide me with abundant financial support.

Thank you all for your kind help again.

References

- [1] Valentina Emilia Balas Anand Nayyar. *International Conference on Innovative Computing and Communications*. Springer-Verlag GmbH, November 2018.
- [2] Sergio C. Capareda. Tidal energy. In *Introduction to Renewable Energy Conversions*, pages 239–264. CRC Press, aug 2019.
- [3] Chris Mi Chun T. Rim. *Wireless Power Transfer for Electric Vehicles and Mobile Devices*. IEEE COMPUTER SOC PR, August 2017.
- [4] B Drew, A R Plummer, and M N Sahinkaya. A review of wave energy converter technology. *Proceedings of the Institution of Mechanical Engineers, Part A: Journal of Power and Energy*, 223(8):887–902, dec 2009.
- [5] John Heidemann, Milica Stojanovic, and Michele Zorzi. Underwater sensor networks: applications, advances and challenges. *Philosophical Transactions of the Royal Society A: Mathematical, Physical and Engineering Sciences*, 370(1958):158–175, jan 2012.
- [6] Jimin Hwang, Neil Bose, and Shuangshuang Fan. AUV adaptive sampling methods: A review. *Applied Sciences*, 9(15):3145, aug 2019.
- [7] Raja Jurdak, Cristina Lopes, and Pierre Baldi. Battery lifetime estimation and optimization for underwater sensor networks. *IEEE Sensor Network Operations*, 05 2006.
- [8] Jugraj Randhawa. Ocean energy: The future of renewable energy. 07 2015.
- [9] Baowei Song, Yushan Wang, Kehan Zhang, and Zhaoyong Mao. Research on wireless power transfer system for torpedo autonomous underwater vehicles. *Advances in Mechanical Engineering*, 10(9):1687814018802563, 2018.

- [10] Peng Zhang Taofeek Orekan. *Underwater Wireless Power Transfer*. Springer-Verlag GmbH, December 2018.
- [11] Ngoc-Huy Tran, Tan-Dat Huynh, Thien-Phuong Ton, and Thai-Hoang Huynh. Design of depth control for hybrid AUV. In *Lecture Notes in Electrical Engineering*, pages 521–531. Springer International Publishing, aug 2020.
- [12] John G. Vlachogiannis. Marine-current power generation model for smart grids. *Journal of Power Sources*, 249:172–174, mar 2014.
- [13] Yushan Wang, Baowei Song, and Zhaoyong Mao. Application of shielding coils in underwater wireless power transfer systems. *Journal of Marine Science and Engineering*, 7(8), 2019.
- [14] Weili Wu, Zhao Zhang, Wonjun Lee, and Ding-Zhu Du. Underwater sensors. In *Optimal Coverage in Wireless Sensor Networks*, pages 257–260. Springer International Publishing, 2020.
- [15] Qingyu Zeng, Jian Ma, Jingwen Mo, and Yan Zhang. Extracting salt difference energy with silicon nitride nanopore generator. In *2020 5th International Conference on Power and Renewable Energy (ICPRE)*. IEEE, sep 2020.